Environmental Fluid Mechanics
https://doi.org/10.1007/s10652-021-09780-y

ORIGINAL ARTICLE

A dry deposition scheme for particulate matter coupled with a well-known Lagrangian Stochastic model for pollutant dispersion

Andrea Amicarelli · Stefano Alessandrini · Giordano Agate · Enrico Ferrero · Guido Pirovano · Gianni Luigi Tinarelli et al. ***[full author details at the end of the article]***

Received: 10 June 2020 / Accepted: 27 January 2021

Abstract
A 3D dry deposition scheme for particulate matter (PM) is presented as a Free-Libre and Open-Source Software (FOSS) library, DePaSITIA (RSE SpA). This combines some advanced formulations for the deposition mechanisms of sedimentation, inertial impaction, turbulent impaction and interception. The scheme also considers bouncing effects. The input quantities relate to the canopy elements (Leaf Area Density, leaf equivalent diameter, leaf shape, orientation and roughness parameters), the transporting fluid (local mean velocity, friction velocity) and the particulate matter (PM local mean concentration, median diameter and density). The deposition scheme is coupled with a well-known Lagrangian Stochastic model for pollutant dispersion, the Open-Source code SPRAY-WEB (Università del Piemonte Orientale et al.). The coupled numerical solution is validated on a laboratory test case representing the dispersion of particulate matter from two line sources within a canopy atmospheric boundary layer. The deposition interfaces are represented by the trees of a scaled spruce forest. Validation refers to the average vertical profile of the deposited mass (not the mean concentration) normalized by the above-canopy mean concentration. Some inter-comparisons are also reported considering uniform Leaf Area Density, the additional effects of molecular diffusion, the height-dependent relative contribution of each deposition mechanism and an alternative deposition scheme. The results of this test case are available as a FOSS tutorial. Considering the Fractional Bias obtained for the deposited mass (FB = 27%), this numerical solution seems suitable to simulating stationary dispersion phenomena within complex canopy boundary layers, assessing the height-dependent dry deposition fluxes of atmospheric PM. The current numerical solution might be improved and applied to elevated obstacles such as electric insulators.

Extended author information available on the last page of the article

Published online: 08 March 2021

Article Highlights

- Development of a height-dependent dry deposition scheme 37 for particulate matter, coupled with a pollutant dispersion code.
- Validation on a vertical profile of deposited pollutant mass.
- Assessment of each deposition mechanism; availability of the code and tutorial as Open-Source Software; possible application to any elevated or ground-level 3D obstacle.

Keywords Dry deposition · Particulate matter · FOSS · DePaSITIA · SPRAY-WEB · Lagrangian stochastic models · Canopy boundary layers · Deposition velocity · Pollutant dispersion

1 Introduction

Deposition processes of the atmospheric particulate matter are relevant in several application fields: impact of atmospheric pollutants on human health; soil, water, forest and food contamination by radioactive or toxic pollutants; vegetation barriers as pollution-control protection actions; contamination of electric insulators; nutrient cycles in the ecosystems; dispersion of pathogenic or GMO spores among crops; forest acidification; conservation of artistic and architectonic works. For a detailed discussion on the application fields interested by dry deposition, we cite the works, among the others, of Petroff et al. [43], Shaw et al. [49] and Ould-Dada et al. [39].

The transfer of a pollutant from the transporting fluid to a solid surface is called deposition. Atmospheric dry deposition takes place in the absence of precipitations. Deposition interests both transported gases and particulate matter. This study exclusively deals with dry deposition of particulate matter. In this case, the following deposition mechanisms are relevant: sedimentation (Sect. 2.3), inertial impaction (Sect. 2.4), turbulent impaction (Sect. 2.5) and interception (Sect. 2.6). In numerical models for air quality, deposition is treated as a sink term in the balance equation of the pollutant mass integrated over a generic computational node. This is a cell in Eulerian models or a particle in Lagrangian models. The numerical modelling of dry deposition for the particulate matter is a key tool to assess the effects of such process on both the concentration fields in the atmospheric domain and the cumulated mass on the deposition surfaces.

In most of the numerical schemes for dry deposition, the deposition flux due to sedimentation includes Stokes' formula for free sedimentation under laminar regime. While the hypothesis of free sedimentation is normally acceptable, except for the applications with high concentrations of particulate matter such as accidents or fires, the hypothesis on the laminar regime is formally not coherent with the motion regimes typical of air quality. However, Stokes' formula is commonly preferred not to deal with the more complex expressions for the limit velocity as function of the drag coefficient. This quantity is dependent on the Reynolds' number Re and the PM particle shape. Particle resuspension is triggered by erosion due to wind or washing, or structural failure of the deposit due to gravity, temperature variations, earthquakes or vibrations. The simulated deposition mass might be zeroed in case of washing. Hereafter some examples of state-of-the-art numerical studies on atmospheric dry deposition are synthesized.

Zhang et al. [57] simulate the effects of dry deposition at the meso-scale. The deposition mechanisms are represented by serial processes, in parallel with sedimentation. The deposition mechanism of turbulent impaction is simplified and refers to the Monin–Obukhov similarity theory [36]. The deposition mechanisms of inertial impaction, molecular diffusion and interception depend on the friction velocity.

Sip and Benes [52] simulate the effects of dry deposition at the micro-scale. The deposition flux due to molecular diffusion depends on Reynolds' number (*Re*). The deposition mechanisms of inertial impaction, molecular diffusion and interception depend on the mean velocity. The deposition mechanisms of interception, inertial impaction and sedimentation depend on the projection of the deposition surface on the plane normal to the mean flow direction. Particle bouncing is neglected: PM particle impingements on the deposition surfaces are considered as completely anelastic.

Dawson et al. [19] assess the dry deposition flux at the micro-scale exclusively in terms of turbulent flux of the transported scalar: they only consider the mechanism of turbulent impaction.

Dry deposition is also treated by sub-grid puff schemes as in CAMx-PiG [14]. It is very simplified dry deposition schemes where deposition velocities are pre-computed constants dependent on the grid cell position and the pollutant species. These processes are activated when the edge of the mean plume intercepts at least one of the barycentres of the grid cells belonging to the lower grid level within the atmospheric domain.

Zhang et al. [58] use the commercial CFD (Computational Fluid Dynamics)—FVM (Finite Volume Method) code FLUENT (2019, Ansys, [10]) to simulate dry deposition of particulate matter on electrical insulators. Their CFD solution is featured by: a RANS (Reynolds-Averaged Navier–Stokes equations) scheme for the transporting fluid; a Lagrangian scheme for the dispersion of particulate matter as a simplified scheme with respect to Lagrangian Stochastic Models; a particle-scale deposition scheme with deposition velocity depending on the mean velocity and the insulator type. Although this study did not present any comparison between numerical results and measures, it might represent one of the first demonstrative examples of dry deposition of particulate matter on electrical insulators.

D'Agostino et al. [17] use a CFD code to study the salt deposit dynamics for the conservation of artistic and architectural works. The deposit is interested by humidity absorbtion and humidity desorption. This can lead to salt solidification (crystallization) and coating of the deposition surface (efflorescence process). Regarding absorption processes, hygroscopy is defined as the physical process by means the deposit absorbs water molecules, whereas deliquescence is the tendency of some salts as $CaCl_2$ to dissolve in the absorbed liquid. These variations in the deposit water content interest the deposit features: depth, temperature, stress status, adhesion and electrical conductance. The following processes are also simulated: dispersion of humidity; phase changes; salt precipitation. In particular, condensation and evaporation are treated as source terms in the continuity equations for the phases.

A sequence of experimental studies on dry deposition is available. Some of them might be also valuable for the validation of numerical models. The following experiments consider flat, horizontal or simplified deposition surfaces or focus on single deposition mechanisms (e.g., Dawson et al. [19]; Vong et al. [56]; Lai and Nazaro [29]; Padro et al. [40]; Petroff et al. [43]; Landis et al. [30]; Gustafson and Franzen [22]; Piskunov [44]; Parker and Kinnersley [41]; Horvath et al. [25]; Adema and Heeres [1]; Huang et al. [26]; Roupsard et al. [48], Calec et al. [13]. Other experimental studies deal with more complex

deposition surfaces such as obstacles or canopies (e.g., Reinap et al. [47]; Pesava et al. [42]; Ould-Dada [38]; Kim et al. [27]).

The current numerical study presents a 3D dry deposition scheme for particulate matter, combining some advanced formulations for the dry deposition mechanisms of inertial impaction, sedimentation, turbulent impaction and interception. Particle bouncing is also simulated. The scheme is sensitive to the main features of the canopy (Leaf Area Density, leaf equivalent diameter, leaf shape, orientation and roughness parameters), the transporting fluid (local mean velocity, friction velocity) and the particulate matter (local mean concentration, median diameter, density). The deposition scheme is coupled with a Lagrangian Stochastic Model for air quality. The coupled numerical solution is validated on a laboratory test case representing the dispersion of particulate matter from two line sources within the canopy atmospheric boundary layer reproduced by Ould-Dada [38]. The deposition interfaces are represented by the trees of a scaled spruce forest. The coupled solution seems able to assess the dry deposition fluxes within complex canopy boundary layers depending on height. The current numerical solution, which is represented by the coupling of the well-known code SPRAY-WEB with the new library DePaSITIA for dry deposition of particulate matter, could also be suitable for dispersion models in urban canopies (e.g., [21]).

The paper is organized as follows: the new deposition scheme and its numerical coupling with SPRAY-WEB are presented (Sect. 2); the test case configuration and the numerical set-up are described (Sect. 3); validation and model inter-comparisons are reported (Sect. 4); the conclusions of the study are summarized (Sect. 5).

2 Depasitia: a dry deposition scheme for particulate matter

DePaSITIA v.1.0 (RSE SpA, [20]) is a dry Deposition scheme for Particulate matter modelling the deposition mechanisms of Sedimentation, Inertial impaction, Turbulent impaction, and Interception, and the process of Adhesion or missing bouncing. As resulting from its full coupling with SPRAY-WEB, DePaSITIA is the only deposition scheme of SPRAY-WEB featured by 3D any-level and multi-level deposition, inertial impaction, turbulent impaction, interception, sensitivity to peculiar input quantities (i.e., non-uniform Leaf Area Density, leaf equivalent diameter and leaf ratios; height-dependent and time-dependent mean velocity; input time-dependent friction velocity).

The mathematical model of DePaSITIA represents an original stand-alone formulation based on pre-existing equations taken from different studies and an analytical solution for time integration of the deposited particle mass. DePaSITIA shares several equations with the advanced dry deposition scheme of Sip and Benes [52], which is implemented in a CFD code. The features discussed in the following differentiate the two schemes.

DePaSITIA is associated with the sectional method, whereas the "state-of-the-art model" of Sip and Benes [52] relies on the moment method. The first approach solves a mass balance equation for each class of the PM particle-size distribution. The latter solves a system of six equations (three mass balances and three moments of the PM particle-size distribution) with six unknowns (three parameters defining the PM particle-size distribution and three moments of the same distribution). The moment method might provide a faster computational speed than the sectional method (with more than three PM classes), but shows the following drawbacks in terms of accuracy: a systematic overestimation of the deposition flux due to inertial impaction; the PM particle-size distribution is assumed as

log-normal; the formulation for Cunningham's coefficient is simplified; the choice of the particle-size distribution moments is arbitrary.

Further, DePaSITIA shows the following advantages, which are absent in the state-of-the-art model: simulation of the adhesion/bouncing effects; potential application to any type of obstacles (the state-of-the-art model introduces assumptions only valid for needle-like obstacles); the analytical formulation newly implemented in SPRAY-WEB for time integration of the deposited particle mass has no truncation error; Lagrangian Stochastic Models (such as SPRAY-WEB) provide several advantages with respect to microscale Reynolds-Averaged Eulerian models for pollutant dispersion ([7]); truncation errors due to time integration for the deposited flux are negligible (Sect. 2.8). On the other hand, DePaSITIA has no deposition mechanism associated with molecular diffusion, which is present in the state-of-the-art model.

The following sub-sections describe: the deposition flux and the balance equation for the mean concentration in the presence of dry deposition (Sect. 2.1); the deposition velocity (Sect. 2.2); the deposition mechanisms of sedimentation (Sect. 2.3), inertial impaction (Sect. 2.4), turbulent impaction (Sect. 2.5) and interception (Sect. 2.6); the adhesion process (Sect. 2.7); the numerical features of the scheme and its coupling with the code SPRAY-WEB (Sect. 2.8).

2.1 Deposition flux and balance equation for the mean concentration

The dry deposition specific flux F_d (kg $\times$ s^{-1} $\times$ m^{-2}) is the deposited mass per unit of time and unit of "horizontal area". The quantity "horizontal area" A_h (m^2) refers to the simple projection of the monitored volume along the horizontal plane. F_d is directly proportional to a particular quantity associated with the specific leaf/vegetation area (i.e., the Leaf Area Density *LAD,* m^{-1}) and the depth of the considered cell Δz (m). Further, F_d is assumed to be linear in concentration. The ratio between F_d and the product of the above quantities (i.e., C, *LAD* and Δz) is an intensive parameter, which is independent on the above quantities and has the dimension of velocity. For this reason, the following ratio is called deposition velocity u_d (m/s, Sect. 2.2):

$$u_d \equiv \frac{F_d}{\overline{C} \cdot LAD \cdot \Delta z} \tag{2.1}$$

where the over-bar symbol denotes Reynolds' ensemble mean and *LAD* is defined as the one-sided area of all the leaf/vegetation surfaces per unit of volume. Other elevated or ground-level deposition surfaces such as ground might be included. The expression "one-sided" means that the intensive quantity *LAD* represents the ratio between the total area of all the external surfaces of vegetation divided by 2 (A_v, m^2) and the associated volume. The deposition on the ground surface can be obtained by properly assessing in the lower layer the input quantities featuring the obstacles, which are not necessarily associated with vegetation in DePaSITIA. However, the deposition on the ground surface is neglected for the test case of Sec. 3, according to the experimental results.

The deposition velocity u_d depends on the instantaneous speed. This means that turbulent fluctuations ([5, 16]) play a non-negligible role in the dispersion of depositing pollutants because the assessment of the pollutant turbulent flux should be required. However, in the present formulation (as in the most advanced deposition models), the Reynolds' mean speed replaces the instantaneous speed.

The specific deposition flux (per unit of horizontal area) is the product between the deposition flux per unit of leaf surface area $F_{d,v}$ (kg $\times$ s^{-1} $\times$ m^{-2}), *LAD* and Δz:

$$F_d = F_{d,v} \cdot LAD \cdot \Delta z \tag{2.2}$$

The product of the Leaf Area Density by the monitoring cell depth can be expressed as follows:

$$LAD \cdot \Delta z = \frac{A_v}{A_h} \tag{2.3}$$

where A_v/A_h is the specific leaf area and can be bigger than the unity, where A_v (m^2) is the one-sided total leaf area within the monitored volume.

The Leaf Area Index (*LAI*) is an extensive quantity equal to the integral of *LAD* over the canopy depth and is not discretized by SPRAY-WEB:

$$LAI = \int_{z=z_g}^{z=h_c} LAD \cdot dz \tag{2.4}$$

where z_g (m) is the ground height and h_c (m) is the height of the canopy top. Provided a certain canopy type such as a conifer forest, *LAI* does not depend on the scale factor if the canopy is uniform. Instead, considering a non-uniform canopy such as a single tree, *LAI* depends on the scale factor.

The deposition flux integrated over the canopy depth $F_{d,ztot}$ (kg $\times$ s^{-1} $\times$ m^{-1}) is the product between the deposition flux per unit area of leaf surface integrated over the canopy depth $F_{d,v,ztot}$ (kg $\times$ s^{-1} $\times$ m^{-1}) and *LAI*:

$$F_{d,ztot} = F_{d,v,ztot} \int_{z=z_g}^{z=h_c} LAD \cdot dz = F_{d,v,ztot} \cdot LAI \tag{2.5}$$

The balance equation for the mean concentration in the presence of dry deposition is expressed as follows:

$$\frac{\overline{dC}}{dt} = -LAD \cdot u_d \cdot \overline{C} \tag{2.6}$$

where t (s) is time. Resuspension modelling (e.g., Hong et al. [24]; Qin et al. [46]) is neglected as in many state-of-the-art studies on dry deposition.

The deposition flux and the deposition velocity are considered Reynolds' averages by definition. In this case the over-bar symbol is omitted just for simplicity of notation.

2.2 Deposition velocity

Assuming dry deposition as the superposition of several independent deposition mechanisms, the deposition velocity can be modelled as follows (Sip and Benes [52]):

$$u_d = R_a(u_{BD} + u_{IN} + u_{IM} + u_{TI} + u_{SE}) \tag{2.7}$$

where "u_{BD}", "u_{IN}", "u_{IM}", "u_{TI}", and "u_{SE}" denote molecular/Brownian diffusion deposition velocity, interception velocity, inertial impaction velocity, turbulent impaction

velocity and sedimentation velocity, respectively. The adhesion coefficient R_a is defined in Zhang et al. [57]. Interception, associated with the mean motion locally tangent to the deposition surface, and turbulent impaction refer to passive PM particles following the streamlines or the trajectories of the fluid particles, respectively. Inertial impaction and sedimentation refer to PM particles continuously detaching from the transporting fluid particles.

Molecular diffusion acts on PM because, even if the molecules of a PM solid particle cannot be interested by a relative motion, they are transported by the air molecules, whose motion is also due to molecular diffusion in the laminar viscous sub-layer. The higher the PM diameter is, the lower the effects of molecular diffusion are. Litschke and Kuttler [31] approximately suggest that deposition due to molecular diffusion is relevant for the PM median diameter $d_{50} < 0.1$ μm. Molecular diffusion is not included in DePaSITIA. Nonetheless some quantifications of its effect on the test case of Sect. 3 are provided in Sect. 4.2.

The dependency of the deposition velocity of each mechanism on the PM median diameter is peculiar: the sedimentation velocity u_{SE} goes with d_{50}^2 (Sect. 2.3), the inertial impaction velocity u_{IN} and the turbulent impaction velocity u_{TI} go with d_{50}^4 for low Stokes numbers (St) and do not depend on d_{50} for high St (Sects. 2.4, 2.5), the interception velocity goes with d_{50} (Sect. 2.6). At the same time, the adhesion coefficient is reduced by the increase of d_{50}, which influences the Stokes number St (Sect. 2.7).

2.3 Sedimentation

Settling velocity u_s (m/s) is approximated by Stokes' equation for the terminal velocity of an isolated spherical particle freely settling under laminar regime, in a fluid initially at rest:

$$u_s = C_C \frac{\rho_{PM} d_{50}^2 g}{18\mu} \tag{2.8}$$

where ρ_{PM} (kg/m^3) is PM density, g (m/s^2) is gravity acceleration and μ (Pa × s) is the dynamic viscosity. Cunningham's correction factor C_c (Hinds [23]) is expressed according to the following relationship (reported in Petroff et al. [43], among the others):

$$C_C = 1 + \frac{2\lambda}{d_{50}} \left(1.257 + 0.4e^{-1.1\frac{d_{50}}{2\lambda}}\right) \tag{2.9}$$

where λ (m) is the mean free path of the particles of the transporting fluid.

Although SPRAY-WEB did not treat settling with a volume term in the balance equation for the pollutant mass, DePaSITIA considers the settling velocity as the boundary term for dry deposition.

The mean free path is expressed as follows:

$$\lambda = \frac{\mu}{\rho} \sqrt{\frac{\pi m_m}{2k_b T}} \tag{2.10}$$

where m_m (kg) is the molecular mass of the transporting fluid, T (K) is temperature and $k_b = 1.380649 \times 10^{-23}$ J/K is the Boltzmann constant.

Under the approximation of ambient conditions, the dynamic viscosity of air is $\mu_{air} = 1.81 \times 10^{-5}$ Pa × s. The air molecular mass is approximated by the molecular mass of dry air: $m_{m,ad} = M_{m,air} \times 10^{-3} / N_A = = 4.82 \times 10^{-26}$ kg, where $N_A = 6.022 \times 10^{23}$ is

Avogadro's constant and M_m = 29.0 g/mol is the molar mass. Air density is ρ_{air} = 1.20 kg/m^3, under the approximation of ambient conditions.

C_C is little dependent on the temperature range in the troposphere (Davies [18]). Thus, temperature in (2.10) is assumed to be T = 293 K.

The fluid-particle contact is a molecule–molecule contact and is perturbed by molecule oscillations. Cunningham's correction factor takes into account that no-slip conditions are not a sufficient approximation for molecular flows, under the domain of statistical mechanics, represented by the Knudsen number $Kn > = 1$. One notices that the following expressions are both valid: $Kn = \lambda / L_{scale}$ and $Kn = \frac{\mathrm{Re}}{Ma}\sqrt{\frac{\pi\gamma}{2}}$. L_{scale} (m) is a proper interaction length scale such as d_{50}; γ is the ratio of the specific heats, Ma is the Mach number. For atmospheric flows, $Kn \approx 1$ in case L_{scale} = ca.10 $\times$ 10^{-6} m. Thus, the dispersion of PM_{10} in atmosphere is affected by Cunnigham's correction factor.

For example, under the hypotheses above, $C_c(d_{50}$ = 10.0 $\times$ 10^{-6} m) = 1.02, $C_c(d_{50}$ = 2.5 $\times$ 10^{-6} m) = 1.07 and $C_c(d_{50}$ = 0.45 $\times$ 10^{-6} m) = 1.37. This value is useful for the test case of Sects. 3, 4.

Sedimentation is the boundary deposition mechanism associate with settling. Sedimentation velocity u_{SE} (m/s) assumes the following form:

$$u_{SE} = u_s k_z,\ k_z \equiv \frac{A_{v,h}}{A_v}, \tag{2.11}$$

where k_z is defined as the ratio between the summation of the projections (over the horizontal plane) of the one-sided areas of each infinitesimal leaf/vegetation element $A_{v,h}$ (m^2) and the one-sided leaf area A_v (m^2) within the same monitored volume. k_z is an intensive non-negative quantity and cannot be bigger than the unity.

2.4 Inertial impaction

Impaction refers to those dry deposition mechanisms where some PM particles detach from the streamlines, due to the particle inertia with respect to the transporting fluid ("inertial impaction") or turbulence ("turbulent impaction"), and impact a deposition surface.

The inertial impaction velocity u_{IM} is expressed as follows (Sip and Benes [52]):

$$u_{IM} = |\overline{u}| k_x E_{IM},\ E_{IM} \equiv \left(\frac{St}{St+\beta}\right)^2,\ k_x \equiv \frac{A_{v,x}}{A_v} \tag{2.12}$$

where the under-bar symbol indicates a vector. The constant β is equal to the average value β = 0.7 (β = 0.6, Sip and Benes [52]; β = 0.8, Zhang et al. [57]). E_{IM} is the efficiency of the inertial impaction mechanism. This efficiency is function of the Stokes number St, a non-dimensional quantity defined as the ratio between the relaxation time τ_p (s) of the motion of a solid particle in a fluid and the characteristic time τ_o (s) of a fluid flow around an obstacle, a PM particle in this context:

$$St \equiv \frac{\tau_p}{\tau_o}, \qquad \tau_o \equiv \frac{d_v}{|\overline{u}|}, \qquad \tau_p \equiv \frac{u_s}{g} \tag{2.13}$$

where d_v (m) is the equivalent leaf diameter. This is here defined as the average value of the geometric mean of the two minor characteristic lengths of each vegetation element (normally a leaf). In case of a needle leaf (Sect. 3), d_v is the leaf diameter.

The higher the Stokes number is, the more intense the particle detachment from the streamlines is. In order words, low St values mean high coherence of the PM particle trajectories with the streamlines.

The leaf ratio k_x is defined as the ratio between the summation of the projections (over the plane normal to the local mean flow direction) of the one-sided areas of each infinitesimal leaf/vegetation element $A_{v,x}$ (m^2) and the one-sided leaf area A_v (m^2) within the same monitored volume. k_x is an intensive non-negative quantity and cannot be bigger than the unity.

One notices that LAD, k_z and k_x are not correlated. LAD expresses the specific leaf area; k_z and k_x quantify the leaf/vegetation shape, roughness and orientation with respect to the mean velocity. For uniform canopies, LAD, k_z and k_x approximately depend on the land-use only and are scale-independent.

2.5 Turbulent impaction

Turbulent impaction is the dry deposition mechanism triggered by the detachment of the particles of the transporting fluid from the streamlines due to turbulence. Under this mechanism, PM particles passively follow the fluid particles.

The turbulent impaction velocity u_{TI} (m/s) is the product of the friction velocity u^* (m/s) by the turbulent impaction efficiency (E_{TI}, Sip and Benes, 2017, [52]):

$$u_{TI} = u_* E_{TI},\ E_{TI} = \left\{ \begin{array}{ll} K_{TI1}(St_t)^2, & St_t < 20 \\ K_{TI2}, & St_t > = 20 \end{array} \right\},$$
$$St_t \equiv \tau_p \frac{\rho u_*^2}{\mu},\ K_{TI1} = 3.5 \times 10^{-4},\ K_{TI2} = 0.18 \tag{2.14}$$

where St_t is the turbulent Stokes' number. This is the ratio between the particle relaxation time and a turbulent time scale. The lower the turbulent time scale is, the higher the intensity of the particle collisions is within the flow. The turbulent Stokes number expresses a measure of the passivity of the PM particles in following the trajectories of the fluid particles, under turbulent regime. One might also consider the turbulent Stokes number as a measure of the inertia of the PM and fluid particles with respect to the streamlines, which are associated with the mean velocity field. Eq. (2.14) shows a discontinuity for St_t = 20.

2.6 Interception

Interception is the dry deposition mechanism of the PM particles which locally follow the streamlines but, due to their non-negligible diameter, are intercepted by the roughness elements of the canopy.

The interception velocity u_{IN} (m/s) is the product of the absolute value of the mean velocity by the leaf ratio k_x and the interception efficiency E_{IN} (Sip and Benes [52]):

$$u_{IN} = |\underline{\overline{u}}| k_x E_{IN}, \qquad E_{IN} \equiv \frac{2d_{50}}{d_v} \tag{2.15}$$

The higher k_x is, the bigger the fluid volume interested by the fluid-leaf interaction is.

2.7 Adhesion/bouncing

The adhesion coefficient R_a is the fraction of PM particles which adhere to the vegetation elements after the interaction with the deposition surfaces, with no bouncing. Following the approximation of Zhang et al. [57], the adhesion coefficient only depends on the Stokes number:

$$R_a = e^{-\sqrt{St}} \tag{2.16}$$

2.8 Numerical features and coupling with SPRAY-WEB

DePaSITIA only focuses on dry deposition. It does not reproduce either the fluid dynamics fields of the transporting fluid or the concentration statistics.

DePaSITIA is coupled with SPRAY-WEB as a library. SPRAY-WEB v.1.0 (2019, Università del Piemonte Orientale et al. [54]; Tinarelli et al. [51]; Alessandrini and Ferrero [4]; Bisignano et al. [12]) is a Lagrangian Stochastic Model for the dispersion of atmospheric pollutants, based on a macromixing scheme. The numerical particles of a generic macromixing scheme (e.g., Minier et al. [35]; Marro et al. [33], Bahlali et al. [11]) represent the motion of a polluted fluid flow during N experimental realizations of the same turbulent phenomenon, under the hypotheses of Reynolds' decomposition. The macromixing scheme of SPRAY-WEB is a simplified variant of Thomson scheme [55] and is based on the assumption that under turbulent regimes, molecular diffusion does not influence the Reynolds' average of the mass balance equation of a passive pollutant (Pope [45]). The same assumption cannot apply to reactive pollutants with 2nd-order kinetics, where an additional scheme for concentration fluctuations is requested (e.g., [3, 7, 32]). It is worth noticing that SPRAY-WEB explicitly works in terms of Lagrangian/particle mass, Eulerian/grid mean concentration and Eulerian/grid mean cumulated deposited mass. Some details on the procedures for dry deposition available in SPRAY-WEB before this study are reported in Alessandrini et al. [2].

DePaSITIA input can be grouped as follows: meteorological input; land-use input; pollutant input.

The input data of DePaSITIA are available in the input files of SPRAY-WEB. Only the mean concentration is calculated by SPRAY-WEB and then provided to DePaSITIA. The format of the meteorological input file of SPRAY-WEB is here generalized to take into account some new variables requested by DePaSITIA, as described in the following.

The meteorological input quantities are the mean velocity vector $\overline{u}(x, y, z, t)$ and the friction velocity of the surface neutral boundary layer just above the canopy $u_*(t)$. For this quantity, horizontal homogeneity is assumed, just for simplicity. The meteorological input values are provided as point values at the edges of the meteorological input grid; they are not located at the centre of the cells. When DePaSITIA is activated, the input mean velocity for the deposition scheme is the vector average of the top and bottom values of each cell.

The land-use input quantities, provided within the meteorological input file of SPRAY-WEB, are $LAD(x, y, z, t)$, $d_v(x, y, z, t)$, $k_x(x, y, z, t)$ and $k_z(x, y, z, t)$. The land-use quantities are discretized with input values formally located at the height of the cell bottom of the input meteorological grid. However, contrarily to the other meteorological input of SPRAY-WEB, the land-use input values for DePaSITIA are not point values, but cell averages, not to be interpolated by SPRAY-WEB.

For each pollutant species, the input quantities for DePaSITIA are $d_{50}(t)$,$\rho_{PM}(t)$ and $\overline{C}(x, y, z, t)$, the latter being produced by the dispersion model.

The dry deposition scheme DePaSITIA is coupled with the Lagrangian Stochastic model SPRAY-WEB v.1.0, which has been improved during the present study both for the coupling with DePaSITIA and for dealing with scaled test cases.

The dry deposition scheme DePaSITIA is activated only for those cells where *LAD* is positive, no matter about the height of the cell barycentre. When DePASITIA is activated, the vertical spatial resolution for the concentration grid of SPRAY-WEB is uniform (Fig. 3).

The coupled solution SPRAY-WEB—DePaSITIA permits the simultaneous deposition of multiple species. For each pollutant, SPRAY-WEB produces both the 2D horizontal field for the Reynolds-averaged time-cumulated deposition mass per unit of horizontal surface $M_{d,2D}$ (kg/m^2) and the 3D field of the quantity $M_{d,*} = M_{d,3D}\Delta z$ (kg/m^2), where $M_{d,3D}$ (kg/m^3) is the Reynolds-averaged time-cumulated deposition mass per unit of volume.

The macromixing time step of SPRAY-WEB v.1.0 has been allowed to be smaller than the unity also to deal with scaled test cases, by generalizing the mutual constraints between the different time scales of the dispersion code.

According to (2.6), the contribution due to dry deposition (symbol $|_d$) to the Lagrangian derivative of concentration is expressed as follows:

$$\left.\frac{dC}{dt}\right|_d = -LAD \cdot u_d \cdot C \tag{2.17}$$

After integration within a generic deposition time step Δt_d(s), one obtains a discretization based on the following analytical solution:

$$C(t + \Delta t_d) = C(t)e^{-(LAD \cdot u_d \cdot \Delta t_d)} \tag{2.18}$$

Following (2.18), the SPRAY-WEB time integration formulation of Anfossi et al. [9] is modified when DePaSITIA scheme isactivated, so that *LAD* replaces the inverse of the depth of the lowest layer of the concentration grid $1/h_1$. This modification also applies to the simplified case with the canopy layer height equal to h_1. In this case DePaSITIA replaces h_1 with h_1/LAI.

In order to minimize the discretization errors in assessing the deposition flux under stationary conditions, the sampling time step Δt_s(s) and the deposition time step are set equal to the macromixing time step. For the same reason, the concentration grid should overlap the meteorological input grid. Under these conditions, the time integration truncation error is negligible in case the following condition is satisfied:$\Delta t_d \leq 0.1s$ (demonstration omitted).

3 Test case configuration and numerical setup

The model coupling SPRAY-WEB—DePaSITIA (Sect. 2) is validated on a laboratory test case representing the dispersion of particulate matter from two line sources within a canopy neutral atmospheric boundary layer (Ould-Dada [38]). The test case configuration and the numerical setup are reported in Sects. 3.1 and 3.2, respectively. More details on the experimental study are available in Ould-Dada [38].

3.1 Test case configuration

The deposition interfaces are the trees of a scale Norway spruce forest. The canopy height is uniform and equal to h_c = 0.450 m. The experimental scale factor is intended to be ca.1:30.

The experimental pollutant sources are represented by two rows of four evenly-spaced point sources covering the whole domain width and located at the inlet section. The heights of these rows (Fig. 7, left panel) are $z_{s,1}$ = 0.700 and $z_{s,2}$ = 0.550 m. No further information is available on the source geometry. The experimental inlet diameter, emission velocity and inlet pollutant flow rate are not available. Then, it is not possible to numerically impose the same inlet conditions as the experiment and the validation cannot refer to the mean concentration field. At the same time, this experiment is one of the very few test cases, maybe the only one, with a vertical profile of the deposition mass, which is divided by the reference concentration at a fixed point. This relative measurement of the deposition mass is reliable as deposition is a linear process in both concentration and velocity.

Both the experimental and simulated data only consider the Uranium mass within the pollutant Uranyl Acetate $UO_2(CH_3 - COO)_2 \cdot H_2O$, an aerosol experimentally emitted from a mixture of salts. The Uranium fraction of the Uranyl Acetate is constant; radioactivity is negligible in assessing the deposition mass for this test case. Under these conditions, the deposition velocity of the Uranium is equal to the deposition velocity of the Uranyl Acetate.

In the experiment, each tree is divided into five uniformly-spaced horizontal layers in order to provide a vertical profile for the deposited mass. Unfortunately, the deposition velocity is not directly available. Instead, the experimental data refer to the following deposition velocity scale $u_{d,*} = \frac{u_d \overline{C}}{\overline{C}_*}$(m/s), where $\overline{C}_*$(kg/m^3) is a concentration scale equal to the mean concentration averaged over 0.450 m $\leq$ z $\leq$ 0.700 m at the outlet section (Ould-Dada [38]).

The validation of Sec. 4 relies on the values of the deposition velocity scale $u_{d,*}$, which is defined in Ould-Dada [38] as the "deposition velocity". Nonetheless, $u_{d,*}$ permits to quantify the deposited mass, which is the main physical quantity involved in the deposition process. The deposition velocity is not the main target. Instead, it is worth noticing that the validation of $\overline{C}$ seems unfeasible for this test case, although many studies on SPRAY-WEB focused on this quantity (SPRAY-WEB [54]). This condition is due both to the lack of experimental information to reproduce the concentration fields and to some probable inconsistencies associated with the relative dispersion profiles in Ould-Dada [38]; ref. columns 3 and 4 of Table 1). Nonetheless, this experiment might be one of the very few studies (probably the only one) reporting an experimental vertical profile of the mass deposited in a canopy layer. It is worth noticing that when defining the deposition velocity

Table 1 Input profile for the leaf area density

z (m)	$LAD \cdot k_z \cdot \Delta z$(Ould-Dada [38])	LAD(m^{-1})
[0.000,0.090]	0.620	31.313
[0.091,0.180]	0.990	50.000
[0.181,0.270]	0.870	43.939
[0.271,0.360]	0.520	26.263
[0.361,0.450]	0.070	3.535

scale, Ould-Dada ([38], Eq. 1) relates to the deposition flux per surface unit, not per tree surface unit.

Ould-Dada [38] states that all the saplings or trees of the "experimental bay", which is a portion the whole wind channel, were sampled except for the last row of trees at the outlet section. He also specifies that 20 saplings out of the 65 saplings of the experiment were sampled. Comparing these statements with the figures of Ould-Dada [38], the monitoring region for the deposition velocity refers to the range 4.000 m $\leq x \leq$ 5.818 m and to the whole domain width.

The experimental friction velocity is $u_* = 0.45$ m/s. However, the results show to be independent on the friction velocity (Sect. 4). Depending on the test case, one or more deposition mechanisms could provide negligible contributions with respect to others.

All the other input data required the pre-processing equations and procedures described in Sect. 3.2.

3.2 Numerical setup

Figure 1 (left panel) shows the input profile elaborated for the mean velocity, according to the available data, which are represented by the point values. The mean velocity is uniform along the horizontal and its unique non-null component is aligned with x-axis. The absolute value of the mean velocity decreases with height in the lowest part of the canopy, is almost linear in the upper part of the canopy, follows a logarithmic profile in the surface neutral boundary layer (just above the canopy top) and tends to a uniform value in the upper part of the wind channel. A simple extrapolation of the mean velocity values applies in the range 1.000 m $\leq z \leq$ 1.200 m, where no data is available and no reconstruction of a top boundary layer is necessary (Sect. 4). Due to the absence of a surface neutral boundary layer at ground (within the canopy; Cassiani et al. [15]-), a linear interpolation is imposed for the mean velocity, instead of the usual logarithmic profile from the similarity theory of Monin and Obukhov [36].

The ensemble standard deviations σ_u (m/s), σ_v (m/s) and σ_w (m/s) of the Eulerian velocity vector $\underline{u} = (u,v,w)$ (m/s) are mandatory input quantities for SPRAY-WEB. As the measured velocities only refer to the components u and w, the experimental turbulence intensity refers to the following 2D quantity:

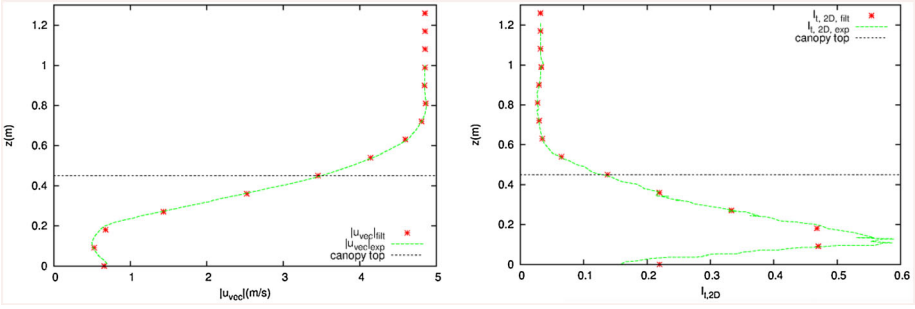

Fig. 1 Profiles of the absolute value of the mean velocity (left panel) and the 2D turbulence intensity (right panel). Digitization of the experimental data (lines) and cell-averaged input (point values). Input pre-processed

$$I_{t,2D} \equiv \frac{\sqrt{\frac{\sigma_u^2+\sigma_w^2}{2}}}{|\underline{u}|} \tag{3.1}$$

Within a neutral boundary canopy layer, the following relationship can be approximately derived from the data of Cassiani et al. [15]:

$$\sigma_u = 1.5\sigma_w \tag{3.2}$$

The system (3.1)–(3.2) provides the following expressions for the standard deviations of the velocity components u and w, as function of the turbulent intensity and the absolute value of the mean velocity:

$$\sigma_u = \frac{3\sqrt{2}}{\sqrt{13}} I_{t,2D}|\underline{u}| \cong 1.18 I_{t,2D}|\underline{u}| \; ; \sigma_w \cong 0.79 I_{t,2D}|\underline{u}| \tag{3.3}$$

The following simplifying hypothesis permits to quantify σ_v:

$$\sigma_v \cong \sigma_w \tag{3.4}$$

This hypothesis is assumed for the input elaboration of σ_v and is removable in case experimental data or meteorological numerical data are available as input for the dispersion model.

Although σ_v had no direct effect on the 2D configuration of the present test case, which is simulated in a 3D domain, (3.4) is necessary to assess the turbulent kinetic energy q (m^2/s^2):

$$q = 1.32\left(I_{t,2D}|\underline{u}|\right)^2, \; I_t \equiv \frac{\sqrt{\frac{\sigma_u^2+\sigma_v^2+\sigma_w^2}{3}}}{|\underline{u}|} \tag{3.5}$$

Figure 1 (right panel) reports the input profile elaborated for the turbulence intensity $I_{t,2D}$. It linearly grows with height in the lower part of the canopy until z = ca.0.12 m, then linearly decreases until the canopy top and exponentially decreases above the canopy tending to a uniform value in the upper part of the wind channel.

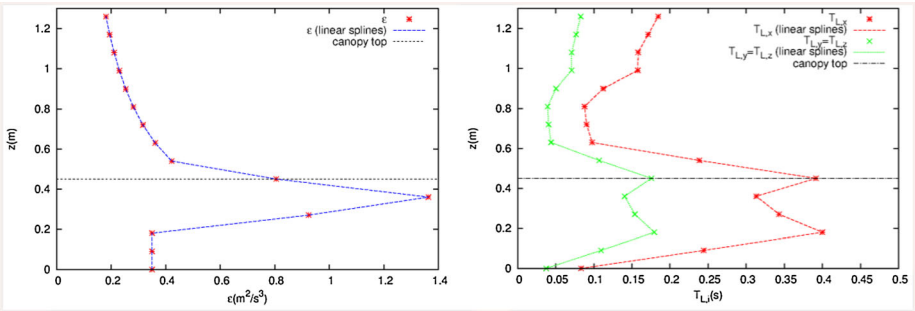

Fig. 2 Profiles of the dissipation rate of the turbulent kinetic energy (left panel) and the components of the Lagrangian integral time scale (right panel). Input pre-processed

The input profile for the dissipation rate of the turbulent kinetic energy ε (m^2/s^3), elaborated as in Fig. 2 (left panel), has a hybrid formulation, as described in the following.

Within the canopy, the following expression is used (Amicarelli et al. 2011b, IJEP [6]):

$$\varepsilon = 0.3q\sqrt{\left(\frac{\partial \overline{u}_k}{\partial x_j}\right)^2} \tag{3.6}$$

where Einstein's notation applies to both the subscripts "$_j$" and "$_k$".

Thomson [55] reports the relationship between the Lagrangian integral time scale $\underline{T}_L$ (s) and the dissipation rate of the turbulent kinetic energy ε m^2/s^3:

$$T_{L,i} = \frac{2\sigma_{u,i}^2}{C_0\varepsilon} \tag{3.7}$$

Equations (3.6)–(3.7) are used within the canopy with the following limiter, derived from the data of Cassiani et al. [15]:

$$T_{L,i}\big|_{z<h_c} \leq 1.05 T_{L,i}\big|_{z=h_c} \qquad \forall i = 1,2,3 \tag{3.8}$$

The limiter (3.8) here imposes the maximum value $\varepsilon_{max} = 0.35 m^2/s^3$ in the lower part of the canopy (Fig. 2, left panel). Above the canopy, the ε profile is approximately expressed by the following formula from the similarity theory of Monin and Obukhov [36] for surface neutral boundary layers, although in a canopy layer this is formally correct only within a limited depth just above the canopy:

$$\varepsilon = \frac{u_*^3}{kz} \tag{3.9}$$

where $k = 0.40$ is the von Karman constant.

The profiles of the components of the Lagrangian integral time scales are reported in Fig. 2 (right panel), elaborated according to (3.7). The maximum absolute values of $\underline{T}_L$ are located in the upper part of the canopy and the values above the canopy are bigger than the canopy bottom.

Kolmogorov constant is set equal to $C_0 = 2$ (Cassiani et al. [15]).

The vertical profile elaborated for *LAD* is reported in Table 1. According to the definitions of Ould-Dada [38], the experimental values of "*LAI*" actually represent the product $LAD \cdot k_z \cdot \Delta z$. The Leaf Ara Density decreases with height according to the typical shape of a spruce, except for the lowest level, which includes both the foliage bottom and the gap between the ground and the foliage. The experimental value of the Leaf Area Index is $LAI = 13.955$.

The leaf ratios are uniform, constant and set equal to $k_z = 0.22$ and $k_x = 0.27$. These values are typical of conifers (Sip and Benes [52]) and scale-independent. The values for k_x and k_z are not provided by Ould-Dada [38]. He states that the vegetation elements of this spruce forest are mainly represented by stems, the conifer little branches, and needles, the conifer leaves, and that stems offer "more potential sites than needles for the adhesion of aerosol particles". Thus, the values of k_x and k_z of the needles of Sip and Benes [52] might present some underestimation for this test case.

The vegetation equivalent diameter is scale-dependent. Its experimental value is unavailable. However, the tree height of the current experiment is known ($h_c = 0.450$ m) together with the leaf size $d_{v,2} = 2$ mm (Sip and Benes [52]) of another conifer tree height

$h_{c,2}$ = 15 m (Sip and Benes, 2017, [52]). Tree allometry (Osada [37]; King [28]) assumes that leaf size scales with tree height by means of the power law $d_v = a h_c^b$. This formula relates the unknown d_v with the available input data: $d_v = d_{v,2}\left(\frac{h_c}{h_{c,2}}\right)^b$. The power law exponent "b" for conifers is sufficient and necessary to estimate d_v for this study, but unfortunately its quantification is unavailable in literature. Nonetheless an expected value of d_v can be assessed. Using the expected value of an input quantity is coherent with estimating the Reynolds' average of the deposited mass. A linear allometric relationship (i.e., b = 1) would provide $d_v = 7 \times 10^{-5}$ m, which has no physical meaning because the leaves of a young spruce such those of the experiment (Shaw et al. [50]; Ould-Dada [38]) are visible to the naked eye. It follows that $b \neq 1$. A power law exponent higher than the unity would provide $d_v < 7 \times 10^{-5}$ m, still losing physical meaning, thus $b < 1$. At the same time, from common experience, the needle diameter of conifers does not decrease with the tree height: $b \geq 0$. From the considerations above, it follows that $b \in [0, 1)$. Without other information, the expected value of the power law coefficient is $E(b) = 0.5$. The needle diameter is then assumed to scale with the root square of the canopy height. This hypothesis implies d_v = 0.36 mm.

The length, width and depth of both the input meteorological domain and the concentration domain of SPRAY-WEB are L_{dom} = 6.000 m, W_{dom} = 3.200 m and H_{dom} = 1.260 m, respectively. Along the vertical, each domain is decomposed in 14 evenly-spaced levels (Sect. 2.8). The length and depth of the numerical domain are equal to the experimental values.

According to the experimental data, the pollutant sources are simulated as two horizontal emission lines, with equal flow rates and barycentres $\underline{x}_{s,1}$=(0.001 m;W_{dom}/2;0.700 m) and $\underline{x}_{s,2}$ = (0.001 m;W_{dom}/2;0.550 m), where W_{dom} (m) is the domain width. The flow rate values are irrelevant for the validation of the deposition velocity scale defined in the following. The sources share the same geometry, featured by L_s = 0.002 m and $A_s = W_{dom} \cdot \Delta z_s$, where Δz_s = 0.002 m is the source depth. The emission time step is very small because it is set equal to the macromixing time step. Two particles per source, released each emission time step, are sufficient to guarantee the solution convergence with respect to the number of numerical particles. The simulated particles are 16,000.

The equivalent aerodynamic diameter is the diameter of an equivalent sphere with liquid water density and same settling velocity as the considered PM species: $d_{a,50}$ = 0.82×10^{-6} m. As the PM density ρ_{PM} = 2920 kg/m^3, one obtains the PM median diameter $d_{50} = 0.45 \times 10^{-6}$ m according to (2.8).

The experimental deposition flux on the ground, which is the bare soil below the canopy, is negligible for this test case [38]. Then, the absence of the settling volume term in SPRAY-WEB, different from the sedimentation boundary term of dry deposition, should not introduce an appreciable error.

Ould-Dada [38] state that the air samplers cover the whole width of the tunnel. This implies that the lateral frontiers of the experimental domain are vertical walls (2D configuration). The numerical value of the domain width is bigger than the experimental value (0.300 m) because SPRAY-WEB does not allow imposing vertical walls at boundaries. Thus, vertical open sections are used as lateral domain frontiers. In order to keep a 2D configuration within the 3D numerical domain, an iterative convergence procedure on W_{dom} was mandatory to make the boundary effects negligible. The domain and the source width are doubled until the fields of the deposition flux and concentration, both averaged over the domain width, converge to stationary conditions. The domain top is treated as an open section. However, this condition has no effect because no numerical particle reaches

that height. The initial conditions are represented by a numerical domain with no numerical particles. Stationary conditions are dynamically achieved. The final physical time of the simulation $t_f = 8$ s is representative of stationary conditions. This time was iteratively chosen to guarantee convergence with respect to stationary conditions.

The spatial resolution of the meteorological input grid along the Cartesian axes are defined by $\Delta x_m = 6.000$ m, $\Delta y_m = W_{dom}$ and $\Delta z_m = 0.090$ m, respectively. The spatial resolution of the statistic grid of SPRAY-WEB along the Cartesian axes are defined by $\Delta x = 0.100$ m, $\Delta y = W_{dom}$ and $\Delta z = 0.090$ m, respectively. No finer resolution is requested to validate the model, provided the spatial resolution of the experimental data available for validation, which is 0.090 m along the vertical. Considered the horizontal homogeneity of the input variables, the concentration grid and the meteorological input grid are practically co-located, thus respecting the condition of Sec. 2.8.

The deposition time step and the sampling time step are chosen to be equal to the minimum value of the macromixing time step ($\Delta t = 0.002$ s) so that the code time discretization guarantees the following condition: $\Delta t = \Delta t_s = \Delta t_d$ (Sect. 2.8).

Both the experimental and numerical data consider velocity and concentration as the cell volume were only filled with air. In other words, the experiment and the numerical model do not consider the effective values of velocity and concentration, depending on the non-null solid volume fractions of the grid cells of the canopy. The effective fluid volume is reduced by the presence of the trees. On the one hand, the experimental data are represented by point values monitored in the fluid sub-domain. On the other hand, the obstacles or vegetation elements are not explicitly simulated (as in [8] and [34]) but their effects are treated as the boundary terms of porous models (e.g., Soares-Frazão et al. [53]). This approach allows not solving explicitly the fluid dynamics fields within the canopy. Instead, a coarser spatial resolution can be applied. In each cell, the fluid terms of the balance equations are weighted by the fluid volume fractions. The canopy boundary terms are weighted on the solid volume fractions associated with the obstacles.

The contribution to the deposition velocity due to molecular/Brownian diffusion is not estimated by DePaSITIA and is here provided by a-posteriori assessment, as explained hereafter.

The Brownian diffusion deposition velocity u_{BD} (m/s) is directly proportional to the absolute value of the local mean velocity (Sip and Benes [52]):

$$u_{BD} = |\overline{\underline{u}}| C_{BD} \frac{\mathrm{Re}^{n_B - 1}}{Sc^{\frac{2}{3}}} \tag{3.10}$$

with the two constants $n_{BD} = 0.5$ and $C_{BD} = 0.467$. Reynolds number (Re) and Schmidt number (Sc) are expressed as follows:

$$\mathrm{Re} = \frac{\rho |\overline{\underline{u}}| d_v}{\mu}, \qquad Sc \equiv \frac{\mu}{\rho D_M} \tag{3.11}$$

In the continuum, the molecular diffusion coefficient D_M (m^2/s) assumes the following expression:

$$D_M = \frac{C_C k_b T}{3\pi\mu d_{50}} \tag{3.12}$$

4 Results

The code SPRAY-WEB, coupled with the deposition scheme DePaSITIA (Sect. 2), reproduces the test case of Sect. 3. The resulting numerical simulation is simply referred as the "reference simulation" of the current study. It is validated in Sect. 4.1 by comparison with the experimental vertical profile of the deposition velocity scale on the test case of Sect. 3. The reference simulation is also compared with a stand-alone SPRAY-WEB simulation using an alternative and pre-existing deposition scheme [54]. Furthermore, the effects of the vertical non-homogeneity of the vegetation are highlighted by a comparison with an alternative simulation with DePaSITIA, assuming a uniform vertical profile for the Leaf Area Density. Finally, the height-dependent relative contributions of each deposition mechanisms in the reference simulation and the effects of molecular diffusion are also analysed (Sect. 4.2).

4.1 Validation and inter-comparisons

The reference simulation is validated on the only experimental vertical profile of the deposited mass and inter-comparisons are reported, as described in the following.

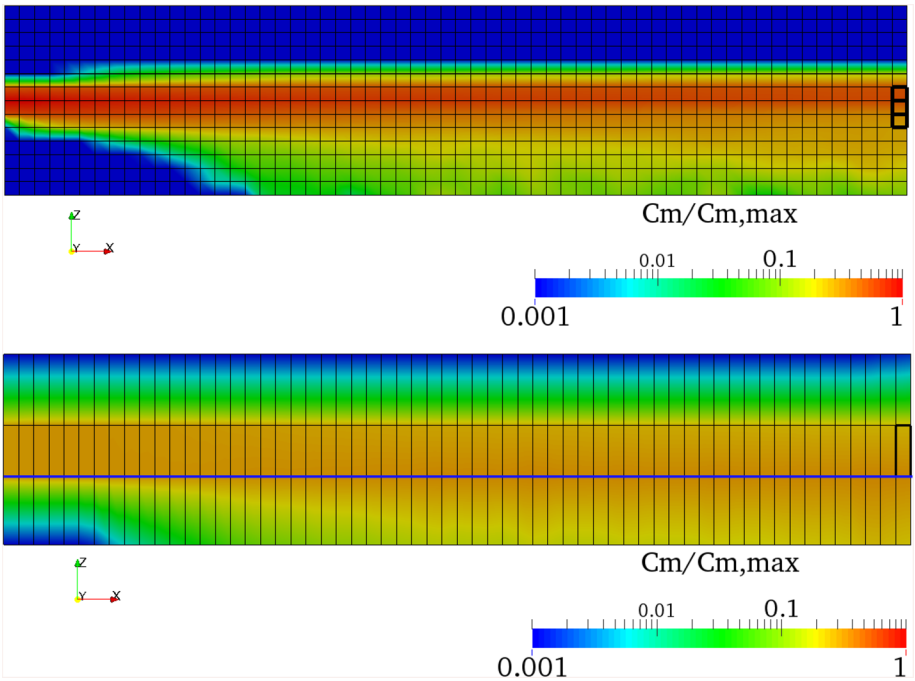

Fig. 3 Stationary fields of the normalized mean concentration. Width-averaged 2D fields. Top panel: reference simulation (SPRAY-WEB and DePaSITIA). Bottom panel: SPRAY-WEB stand-alone simulation. Without DePaSITIA the canopy cannot be partitioned in vertical levels. The above quantities are normalized by the maximum value of the field of the reference simulation. The cells belonging to the monitoring regions of the mean concentration scale are highlighted in the top panel (3 cells at the outlet section, just above the canopy) and in the bottom panel (1 cell), respectively

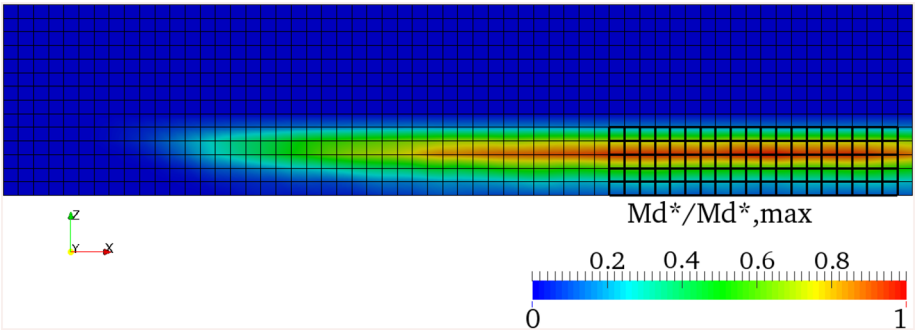

Fig. 4 Field of the normalized values of $M_{d,*}$ (the product of the cell depth times the Reynolds-averaged time-cumulated deposition mass per unit of volume) at $t = t_f$. Width-averaged 2D field of the reference simulation (with SPRAY-WEB and DePaSITIA). $M_{d,*}$ is normalized by its maximum value. The cells belonging to the monitoring regions of the deposition mass are highlighted in the most downstream part of the canopy (except for the outlet section). The SPRAY-WEB stand-alone simulation (without DePaSITIA) does not provide any height-dependent field of the deposited mass

Figure 3 (top panel) shows the stationary field of the concentration mean. At the spatial resolution of the statistic grid, the two source plumes approximately appear as a unique plume emitted from an Elevated Source. The centreline of this plume is described by the local maxima along the vertical, as function of the distance from the inlet section. This line shifts towards the emission height of the upper pollutant source. The plume is more dispersed within the canopy due to higher turbulence and lower mean velocity values than above the canopy. The monitoring region of the mean concentration scale is highlighted at the outlet section, above the canopy. The plume begins to interact with the ground upstream the monitoring region of the deposited mass, which is in turn highlighted in Fig. 4. The same simulation is also reproduced by SPRAY-WEB v.1.0 using a simplified deposition scheme for particulate matter, alternative to DePaSITIA (Fig. 3, bottom panel). The simplified scheme provides a uniform and constant deposition velocity depending on the land-use type and can only work in the lowest vertical level, thus constraining the spatial resolution of the whole numerical concentration grid. Nonetheless, this SPRAY-WEB stand-alone solution takes advantage from those minor code modifications which are independent from DePaSITIA and are mandatory to apply SPRAY-WEB v.1.0 to scaled test cases, as mentioned in Sect. 2.8. The land-use type for the simplified deposition scheme is associated with a pre-defined value of friction velocity, which is the only quantity influencing the deposition velocity of this scheme. The land-use type is chosen to provide the input friction velocity as close as possible to the experimental value.

The deposition quantity $M_{d,*}$ (kg/m^2) is the product of the cell depth times the Reynolds-averaged time-cumulated deposition mass per unit of volume. $M_{d,*}$ ($t = t_f$) is reported in Fig. 4. The vertical evolution of $M_{d,*}$ is influenced by the variation of the mean velocity, the mean concentration and the Leaf Area Density. Both $|\overline{u}|$ and $\overline{C}$ approximately grow with height within the canopy. On the other hand, *LAD* decreases with height, except for the first level. The overall effect is a general growth of $M_{d,*}$ with height, but the upper canopy level where *LAD* reaches its minimum level within the canopy. The longitudinal evolution of $M_{d,*}$ is only due to the variation of the mean concentration field, with a general growth of $M_{d,*}$ with the distance from the source with a slight decrease close to the outlet section at every canopy level. This pattern is confirmed by the longitudinal profiles of the Reynolds-averaged time-cumulated deposition mass per unit of horizontal area ($M_{d,2D}$, kg/

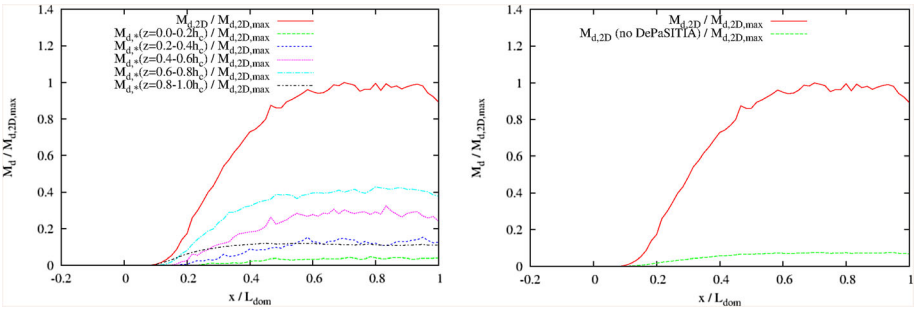

Fig. 5 Left panel. Longitudinal profile of the Reynolds-averaged time-cumulated deposition mass per unit of horizontal area $M_{d,2D}$ at $t = t_f$ and its height-dependent contributions $M_{d,*}$. Width-averaged values. All the values are normalized by the maximum value of $M_{d,2D}$. Right panel: comparison between the reference simulation (with SPRAY-WEB and DePaSITIA) and the SPRAY-WEB stand-alone simulation (without DePaSITIA there is no local height-dependent contribution)

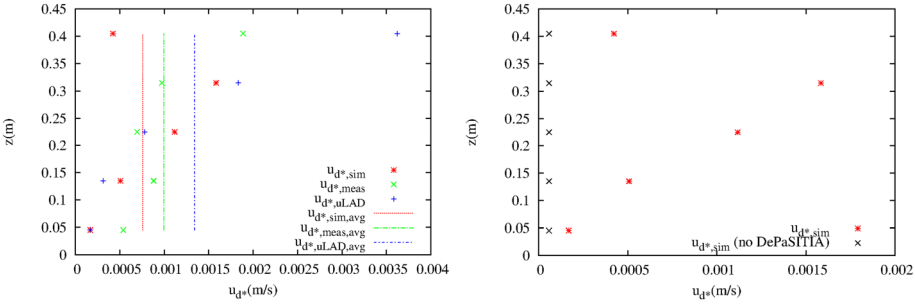

Fig. 6 Vertical profiles of the deposition velocity scale. Left panel: comparisons between the available measures ("$_{meas}$") and the numerical results considering both the reference simulation ("$_{sim}$") and an alternative variant with uniform *LAD* within the canopy ("$_{uLAD}$"). Width-averaged values. Right panel: comparison between the reference simulation (with SPRAY-WEB and DePaSITIA) and the SPRAY-WEB stand-alone simulation (without DePaSITIA there is no dependence on height)

m^2) at $t = t_f$ and its canopy-level contributions (Fig. 5, left panel). The deposition cumulated mass grows with height within the canopy, no matter about the distance from the source, except for the canopy top level, whose relative mass decreases with x. It is worth noticing that the simplified scheme alternative to DePaSITIA does not allow SPRAY-WEB to produce such height-dependent fields of the deposited mass. Figure 5 (right panel) reports the comparisons between the longitudinal profiles of the deposited mass for the reference simulation (SPRAY-WEB and DePaSITIA) and the SPRAY-WEB stand-alone simulation, which systematically provides underestimations of one order of magnitude.

Figure 6 (left panel) shows the comparisons between the simulated profiles of the deposition velocity scale and the available measurements. The reference numerical simulation (subscript "$_{sim}$") provides a reasonable assessment of the deposition velocity scale. The profile shape is similar to the experimental profile, with an increase of $u_{d,*}$ with height, but the top canopy level, where a relevant underestimation is recorded. This discrepancy seems related to the vertical variation of the Leaf Area Density: the additional profile of the deposition velocity scale obtained with a uniform *LAD* shows a shape more similar to the experimental one. The simulated deposition velocity scale averaged over the canopy depth

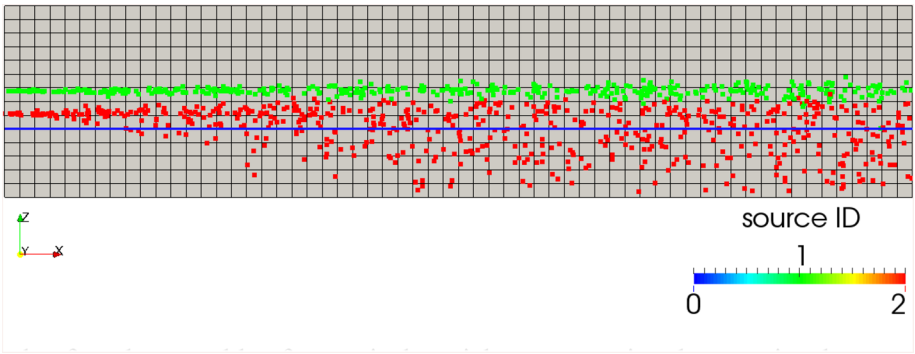

Fig. 7 Example of a sub-ensemble of numerical particles representing the associated source under stationary conditions. Lateral view. The blue horizontal line represents the canopy top

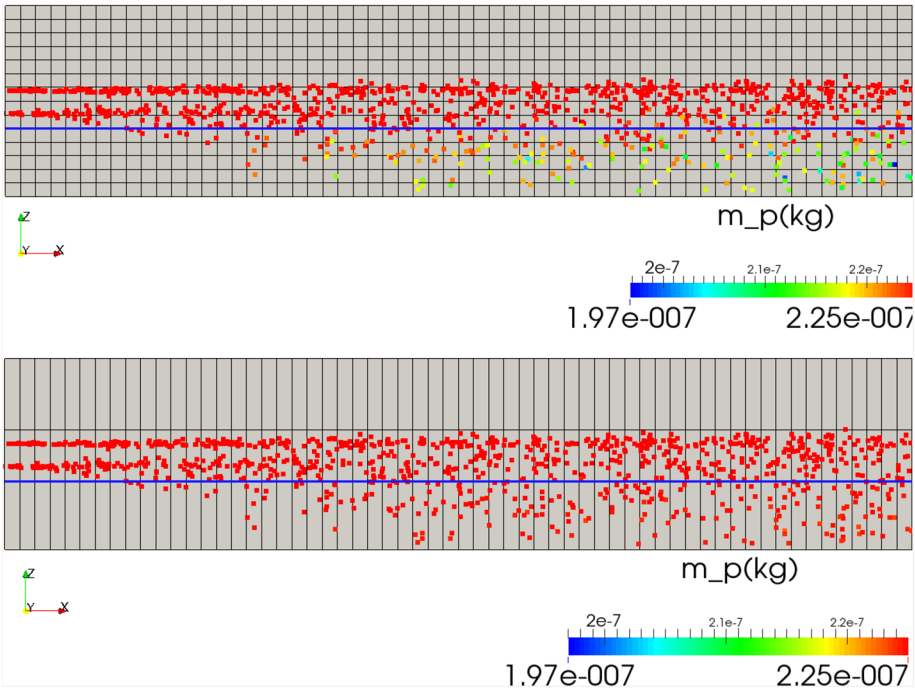

Fig. 8 Example of a sub-ensemble of numerical particles representing the particle pollutant mass under stationary conditions. Lateral views. The blue horizontal line represents the canopy top. Top panel: reference simulation (with SPRAY-WEB and DePaSITIA). Bottom panel: SPRAY-WEB stand-alone simulation (without DePaSITIA)

$u_{d,*,sim,avg} = 7.599 \times 10^{-4}$ m/s provides an underestimation of 24%, with respect to the experimental value $u_{d,*,meas,avg} = 9.952 \times 10^{-4}$ m/s. The simulation with uniform *LAD* provides $u_{d,*,uLAD,avg} = 1.342 \times 10^{-3}$ m/s, with an overestimation of 35%.

Figure 6 (right panel) reports the comparisons between the vertical profile of the deposited mass for the reference simulation and the SPRAY-WEB stand-alone results, which are featured by a uniform deposition velocity, maximum underestimations of two orders of magnitude and an average deposited mass of 7.4% the average of the reference simulation.

Figure 7 reports a sub-ensemble of numerical particles representing the associated source under stationary conditions. At the finer scale of the macromixing scheme the two source plumes are almost completely segregated. The SPRAY-WEB stand-alone solution provides the same particle trajectories as the reference simulation as the deposition scheme does not affect the macromixing scheme.

The same particle sub-ensemble is used to show an example distribution of the particle pollutant mass m_p (kg) (Fig. 8 bottom panel). This quantity is uniform above the canopy and decreases with the distance from the inlet section within the canopy as each particle loses some pollutant mass during each time step spent within the canopy, where dry deposition occurs. The vertical distribution of m_p within the canopy is complex and depends on both the vertical variation of the deposition velocity and the particle trajectory. It is worth noticing that the mass m_p of a numerical particle is an instantaneous-like quantity, not a Reynolds' average. The maximum consumption of the particle pollutant mass due to dry deposition is ca.12%. With respect to the reference simulation, the SPRAY-WEB stand-alone results (Fig. 8 top panel) underestimate the deposited mass so that no relevant reduction in the particle pollutant mass is recorded and the maximum pollutant mass consumption is ca.1%.

4.2 Analysis of the contributions of the deposition mechanisms

The vertical profiles for each dry deposition mechanism are reported both as absolute values (Fig. 9) and percentages (Table 2). Unfortunately, there is no measurement to validate these particular estimations. Interception and inertial impaction are responsible for 87% and 9% of dry deposition, respectively. Sedimentation, turbulent impaction and molecular diffusion are negligible at any canopy level. Thus, the friction velocity and the

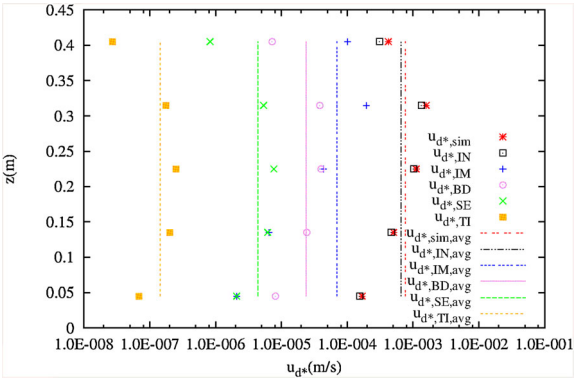

Fig. 9 Vertical profiles of the contribution to the deposition velocity scale for each deposition mechanism, including the a-posteriori assessment of the Brownian diffusion deposition velocity

Table 2 Vertical profiles of the adhesion coefficient and of the percentage contributions of each deposition mechanism to the deposition velocity. Width-averaged values

	$0.000 \leq z \leq 0.090$	$0.091 \leq z \leq 0.180$	$0.181 \leq z \leq 0.270$	$0.271 \leq z \leq 0.360$	$0.361 \leq z \leq 0.450$	$0.000 \leq z \leq 0.450$
$\frac{u_{SE} \cdot R_a}{u_d} \cdot 100$	1.24	1.22	0.69	0.34	0.20	0.59
$\frac{u_{IM} \cdot R_a}{u_d} \cdot 100$	1.25	1.29	3.88	12.38	24.15	9.15
$\frac{u_{TI} \cdot R_a}{u_d} \cdot 100$	0.04	0.04	0.02	0.01	0.01	0.02
$\frac{u_{IN} \cdot R_a}{u_d} \cdot 100$	92.64	92.66	91.82	84.85	73.93	87.12
$\frac{u_{BD} \cdot R_a}{u_d} \cdot 100$	4.83	4.80	3.59	2.42	1.72	3.12
R_a	0.94	0.94	0.92	0.89	0.87	0.90

leaf ratio k_z are the only input quantities (Sec. 2.8) that do not affect the results. Interception is the major deposition mechanism for this test case. The contribution of molecular diffusion is around one order of magnitude smaller than interception, no matter about height. The same relationship approximately stands for sedimentation and molecular diffusion, and for turbulent impaction and sedimentation. Each mechanism velocity increases with height until a local maximum at the third or fourth level and a local or absolute minimum at the top level. Inertial impaction has a stronger variation with height: at the lowest level, it provides a deposition velocity close to sedimentation, whereas at the top level it is of the same order of magnitude as interception. Inertial impaction contribution grows with height and is only relevant in the fourth and the top level, with 12% and 24% of the local deposited mass, respectively. Within the lowest three canopy levels, interception is the only appreciable mechanism providing 92–93% of the deposited mass. The adhesion coefficient decreases with height. Its minimum, average and maximum values are $R_{a,min} = 0.87$, $R_{a,avg} = 0.90$ and $R_{a,max} = 0.94$, respectively.

5 Conclusions

The main conclusions of this study can be synthesized as follows: one of the very few height-dependent dry deposition scheme for particulate matter is developed for both height-varied and height-uniform vegetation canopies; the proposed deposition scheme is coupled with a well-known pollutant dispersion code; the resulting validation on a vertical profile of deposited mass might represent a novelty in literature; the relative contribution of each deposition mechanism of the scheme is highlighted; the reference code and the tutorial of the present test case are available as Open-Source Software; the deposition scheme is based on advanced CFD deposition mechanisms, might be further applied to any elevated or ground-level 3D obstacle in the atmosphere and seems suitable to coupling with both meso-scale and micro-scale air quality models. Further details are discussed hereafter.

A 3D dry deposition scheme for particulate matter is presented as a FOSS (Free-Libre and Open-Source Software) library, which is DePaSITIA (RSE SpA). This combines some advanced formulations for the deposition mechanisms of sedimentation, inertial impaction, turbulent impaction and interception. The bouncing effects are also considered by means of the adhesion coefficient. The scheme is sensitive to some major quantities featuring the transporting fluid (local mean velocity, friction velocity), the canopy (Leaf Area Density, leaf equivalent diameter, two leaf ratios depending on the leaf shape, orientation and roughness), and the particulate matter (local mean concentration, median diameter, density). The deposition scheme is coupled with a Lagrangian Stochastic model for pollutant dispersion, the Open-Source code SPRAY-WEB (Università del Piemonte Orientale et al.). The coupled numerical solution is validated on a laboratory test case representing the dispersion of particulate matter from two line sources within a canopy simulated boundary layer (Ould-Dada [38]). The deposition interfaces are represented by the trees of a scaled spruce forest. Validation refers to the average vertical profile of the deposited mass, not the mean concentration, normalized by the above-canopy mean concentration. The numerical average value of the deposition velocity scale within the canopy seems close enough to the experimental value, with an underestimation of 24% and a Fractional Bias of 27%. The

numerical profile shape is similar to the measured curve: the deposition velocity scale increases with height, but a relevant underestimation is recorded at the top canopy level. This discrepancy seems related to the vertical variation of the Leaf Area Density as an additional numerical profile, obtained with an average value for the Leaf Area Density, shows a shape more similar to the experimental curve, despite bigger errors in terms of absolute values. The 2D deposition field of the product of the cell depth times the Reynolds-averaged time-cumulated deposition mass per unit of volume is reported. Some inter-comparisons are also shown considering uniform Leaf Area Density, the additional effects of molecular diffusion, and the relative contribution of each deposition mechanism depending on height. The maximum consumption of a generic particle pollutant mass due to dry deposition is ca.12%.

The same simulation is also reproduced using SPRAY-WEB v.1.0 with a simplified deposition scheme for particulate matter, alternative to DePaSITIA. The alternative scheme assumes a uniform and constant pre-defined deposition velocity depending on the land-use type and can only work in the lowest vertical level, thus constraining the spatial resolution of the whole numerical concentration grid. With respect to the SPRAY-WEB stand-alone results, the reference simulation of the current study computes height-dependent deposition velocity fields and avoids maximum underestimations of two orders of magnitude and average underestimations of ca.93%.

The numerical results of this test case are also available as a FOSS tutorial on the SPRAY-WEB repository.

The numerical coupling of the Lagrangian Stochastic Model SPRAY-WEB with the deposition scheme DePaSITIA seems suitable to simulate stationary dispersion phenomena within complex canopy boundary layers assessing the height-dependent deposition fluxes of particulate matter. The numerical solution of this study might also be investigated under non-stationary regimes.

Appendix A: lists of acronyms and symbols

See Tables 3, 4.

Table 3 List of acronyms

Acronym	Description	Acronym	Description
CFD	Computational fluid dynamics	FVM	Finite volume method
FD	Finite difference method	PM	Particulate matter
FOSS	Free-libre and open-source software	RANS	Reynolds-averaged Navier–Stokes

Table 4 List of symbols

Symbol	Quantity	Symbol	Quantity
$\underline{\cdot}$ (Under-bar)	Vector notation	n_{BD}	Diffusion deposition constant
$\overline{\cdot}$ (Over-bar)	Reynolds' ensemble mean	PM_{10}	PM with diameter smaller than 10 μm
a	Tree allometry power-law constant	q (m^2/s^2)	Turbulent kinetic energy
A_h (m^2)	Leaf "horizontal area"	R_a	Adhesion coefficient
A_s (m^2)	Source area	Re	Reynolds' number
A_v (m^2)	one-sided total Leaf/obstacle area within a given volume	Sc	Schmidt number
$A_{v,h}$ (m^2)	horizontal projection of The upward elements of A_v	St	Stokes numbers
$A_{v,x}$ (m^2)	Normal projection of the leeward elements of A_v	St_t	Turbulent Stokes' number
A_v/A_h	Specific leaf area	T (K)	Temperature
b	Allometry power-law constant	t (s)	Time
C (kg/m^3)	Concentration	t_f(s)	Final physical time of the simulation
C_* (kg/m^3)	Test-case dependent Concentration scale	$\underline{T_L}$ (s)	Lagrangian integral time Scale vector
C_0	Kolmogorov constant	u^* (m/s)	Friction velocity
$CaCl_2$	Calcium chloride	$\underline{u}$ = (u,v,w) (m/s)	Eulerian velocity vector
C_{BD}	Diffusion deposition constant	u_{BD} (m/s)	molecular/Brownian Diffusion deposition velocity
C_c	Cunningham's correction factor	u_d (m/s)	Deposition velocity
d_{50} (m)	PM median diameter	$u_{d,*}$ (m/s)	Test-case dependent deposition velocity scale
$d_{a,50}$ (m)	Equivalent aerodynamic d_{50}	$u_{d,*,meas,avg}$ (m/s)	Experimental $u_{d,*}$ averaged over the canopy depth
D_M (m^2/s)	Molecular diffusion coefficient	$u_{d,*,sim,avg}$ (m/s)	Simulated $u_{d,*}$ averaged over the canopy depth
d_v (m)	Equivalent leaf diameter or leaf diameter or travel characteristic length of the obstacle	$u_{d,*,uLAD,avg}$ (m/s)	$u_{d,*,sim,avg}$ under uniform LAD
E_{IM}	INERTIAL impaction efficiency	u_{IM} (m/s)	Inertial impaction velocity
E_{IN}	Interception efficiency	u_{IN} (m/s)	Interception velocity
E_{TI}	Turbulent impaction efficiency	$UO_2(CH_3-COO)_2{\cdot}H_2O$	Uranyl Acetate
F_d ($kg \times s^{-1} \times m^{-2}$)	Dry deposition specific flux	u_s (m/s)	Settling velocity
$F_{d,IN}$ ($kg \times s^{-1} \times m^{-2}$)	Interception deposition flux	u_{SE} (m/s)	Sedimentation velocity

Table 4 continued

Symbol	Quantity	Symbol	Quantity
$F_{d,v}$ (kg × s^{-1} × m^{-2})	Deposition flux per unit of leaf area	u_{TI} (m/s)	Turbulent impaction velocity
$F_{d,ztot}$ (kg × s^{-1} × m^{-1})	Deposition flux integrated over the canopy depth	W_{dom} (m)	Domain width
g (m/s^2)	Gravity acceleration	$\underline{x} = (x,y,z)$ (m)	Eulerian position vector
h_1(m)	Depth of the lowest layer of the concentration grid	x_s (m)	source position along x-axis
h_c (m)	Canopy depth	z_g (m)	Ground height
H_{dom} (m)	domain depth	$z_{s,i}$ (m)	Height of the i-th source
$I_{t,2D}$	Turbulence intensity (2D formulation)	Δt (s)	Macromixing time step
k	von Karman constant	Δt_d (s)	Deposition time step
k_b (J/K)	Boltzmann constant	Δt_s (s)	Sampling time step
Kn	Knudsen number	$\Delta \underline{U}$ (m/s)	Velocity increment vector
k_x	leaf/obstacle ratio Between $A_{v,x}$ and A_v in a given volume	Δx (m)	spatial resolution of the Concentration grid along x-axis
k_z	Leaf/obstacle ratio Between $A_{v,h}$ and A_v in a given volume	Δx_m (m)	Spatial resolution of the Meteorological input grid along x-axis
LAD	Leaf area density or Local specific surface of the obstacle	Δy (m)	Spatial resolution of the concentration grid along y-axis
LAI	Leaf Area Index	Δy_m (m)	Spatial resolution of the meteorological input grid along y-axis
L_{dom} (m)	Domain length	Δz (m)	Spatial resolution of the concentration grid along z-axis
L_s (m)	Source length	Δz_m (m)	Spatial resolution of the meteorological input grid along z-axis
L_{scale} (m)	Sedimentation length scale	β	Inertial impaction constant
Ma	Mach number	ε (m^2/s^3)	DISSIPATION rate of the turbulent kinetic energy
$M_{d,*}$ (kg/m^2)	Cell depth times Reynolds-averaged Time-cumulated deposition mass per unit of volume	γ	Ratio of the specific heats

Table 4 continued

Symbol	Quantity	Symbol	Quantity
$M_{d,2D}$ (kg/m^2)	Reynolds-averaged Time-cumulated deposition mass per unit of horizontal area	λ (m)	Mean free path of the particles of the transporting fluid
$m_{m,ad}$ (kg)	Molecular mass of dry air	μ (Pa × s)	Dynamic viscosity
$M_{m,air}$ (g/mol)	Air molar mass	ρ (kg/m^3)	Density
m_p (kg)	pollutant mass of a Generic numerical particle	σ_u (m/s), σ_v (m/s), σ_w (m/s)	Ensemble standard deviations of the Eulerian velocities
N	Number of realizations of the turbulent phenomenon	τ_o (s)	Characteristic time of a fluid flow around an obstacle
N_A	Avogadro's constant	τ_p (s)	Relaxation time of the motion of a solid particle in a fluid

Acknowledgements The contributions of the RSE authors have been financed by the Research Fund for the Italian Electrical System (for "Ricerca di Sistema -RdS-"), in compliance with the Decree of Minister of Economic Development April 16, 2018. The software library "DePaSITIA v.1.0" has been financed by the Research Fund for the Italian Electrical System (for "Ricerca di Sistema -RdS-") under the Contract Agreements between RSE SpA and the Italian Ministry of Economic Development, in compliance with the Decree of Minister of Economic Development April 16, 2018 (and analogous following agreements). The RSE contributions to SPRAY-WEB v.1.0 (Università del Piemonte Orientale et al.) were realised thanks to the funding 'Fondo di Ricerca per il Sistema Elettrico' within the frame of Program Agreements between RSE SpA and the Italian Ministry of Economic Development (Ministero dello Sviluppo Economico). The contributions of S. Alessandrini to the current study were made before January 2014 as an employee of RSE SpA, except for the manuscript's co-revision carried out under his current affiliation at NCAR. The first author is thankful to Prof. George Shaw (University of Nottingham, UK) for his advices during a preliminary stage of the current study.

References

1. Adema EH, Heeres P (1995) Dry deposition of sulphur dioxide and ammonia on wet surfaces and the surface oxidation kinetics of bisulphite. Atmos Environ 29(10):1091–1103
2. Alessandrini S, Pirovano G, Costa MP, Ferrero E, Belfiore G (2005) Deposizione e trasformazione chimica degli inquinanti in un modello di dispersione lagrangiano; Rapporto CESI n° A5053302
3. Alessandrini S, Ferrero E (2011) A Lagrangian particle model with chemical reactions: application in real atmosphere. Int J Environ Pollut 47:97–107
4. Alessandrini S, Ferrero E, Anfossi D (2013) A new Lagrangian method for modelling the buoyant plume rise. Atmos Environ 77:239–249
5. Amicarelli A, Leuzzi G, Monti P, Thomson DJ (2011) A comparison between IECM and IEM Lagrangian models. Int J Environ Pollut 44(1/2/3/4):324–331
6. Amicarelli A, Leuzzi G, Monti P, Thomson DJ (2011) LAGFLUM, a stationary 3D Lagrangian stochastic numerical micromixing model for concentration fluctuations: validation in canopy turbulence, on the MUST wind tunnel experiment. Int J Environ Pollut 47(n.1/2/3/4):317–325
7. Amicarelli A, Leuzzi G, Monti P, Alessandrini S, Ferrero E (2017) A stochastic Lagrangian micromixing model for the dispersion of reactive scalars in turbulent flows: role of concentration fluctuations and improvements to the conserved scalar theory under non-homogeneous conditions. Environ Fluid Mech 17(4):715–753. https://doi.org/10.1007/s10652-017-9516-1
8. Andronopoulos S, Grigoriadis D, Robins A, Venetsanos A, Rafailidis S, Bartzis JG (2001) Three-dimensional modelling of concentration fluctuations in complicated geometry. Environ Fluid Mech 1(4):415–440

9. Anfossi D, Sacchetti D, Trini Castelli S (1995) Development and sensitivity analysis of a Lagrangian particle model for long range dispersion. Env Soft 10–4:263–287
10. Ansys Fluent. https://www.ansys.com/products/fluids/ansys-fluent. Access 15 Nov 2019
11. Bahlali ML, Dupont E, Carissimo B (2019) Atmospheric dispersion using a Lagrangian stochastic approach: application to an idealized urban area under neutral and stable meteorological conditions. J Wind Eng Ind Aerodyn 193:103976. https://doi.org/10.1016/j.jweia.2019.103976
12. Bisignano A, Mortarini L, Ferrero E, Alessandrini S (2017) Model chain for buoyantplume dispersion. Int J Environ Pollut 62(2/3/4):200–213
13. Calec N, Boyer P, Anselmet F, Amielh M, Branger H, Mailliat A (2017) Dry deposition velocities of submicron aerosols on water surfaces: laboratory experimental data and modelling approach. J Aerosol Sci 105:179–192
14. CAMx v.6.10 (ENVIRON Int. Corp.); http://www.camx.com/download/default.aspx
15. Cassiani M, Radicchi A, Albertson J (2007) Modelling of concentration fluctuations in canopy turbulence. Bound-Layer Meteorol 122:655–681
16. Contini D, Robins AG, Hayden P (2014) Statistical properties of concentration fluctuations in two merging plumes. Environ Fluid Mech 14(4):919–942
17. D'Agostino D, Congedo PM, Cataldo R (2014) Computational fluid dynamics (CFD) modeling of microclimate for salts crystallization control and artworks conservation. J Cult Herit 15(4):448–457
18. Davies C (1945) Definitive equations for the fluid resistance of spheres. Proc Phys Soc 57:259
19. Dawson M, Borman D, Hammond BR, Lesnic D, Rhodes D (2014) Moving boundary models for the growth of crystalline deposits from undetected leakages of industrial process liquors. Comput Chem Eng 71:331–346
20. DePaSITIA v.1.0 (RSE SpA); 2019; https://github.com/AndreaAmicarelliRSE/DePaSITIA
21. Efthimiou GC, Andronopoulos S, Tolias I, Venetsanos A (2016) Prediction of the upper tail of concentration distributions of a continuous point source release in urban environments. Environ Fluid Mech 16(5):899–921
22. Gustafsson MER, Franzén LG (1996) Dry deposition and concentration of marine aerosols in a coastal area, SW Sweden. Atmos Environ 30(6):977–989
23. Hinds W (1999) Aerosol technology: properties, behavior, and measurement of airborne particles, 2nd edn. Wiley, Hoboken
24. Hong B, Lin B, Qin H (2017) Numerical investigation on the effect of avenue trees on PM2.5 dispersion in urban street canyons. Atmosphere. https://doi.org/10.3390/atmos8070129
25. Horvath L, Nagy Z, Weidinger T (1998) Estimation of dry deposition velocities of nitric oxide, sulfur dioxide, and ozone by the gradient method above short vegetation during the TRACT campaign. Atmos Environ 32(7):1317–1322
26. Huang J, Liu Y, Holsen TM (2011) Comparison between knife-edge and frisbee-shaped surrogate surfaces for making dry deposition measurements: wind tunnel experiments and computational fluid dynamics (CFD) modelling. Atmos Environ 45:4213–4219
27. Kim E, Kalman D, Larson T (2000) Dry deposition of large, airborne particles onto a surrogate surface. Atmos Environ 34:2387–2397
28. King DA (1991) Tree allometry, leaf size and adult tree size in old-growth forestsof western Oregon. Tree Physiol 9:369–381
29. Lai ACK, Nazaro WW (2000) Modeling indoor particle deposition from turbulent flow onto smooth surfaces. J Aerosol Sci 31(4):463–476
30. Landis MS, Keeler GJ, Al-Wali KI, Stevens RK (2004) Divalent inorganic reactive gaseous mercury emissions from a mercury cell chlor-alkali plant and its impact on near-field atmospheric dry deposition. Atmos Environ 38:613–622
31. Litschke T, Kuttler W (2008) On the reduction of urban particle concentration by vegetation—a review. Meteorol Z 17:229–240
32. Lo Iacono G (2009) Application of Rice's theory to recurrence statistics of concentration fluctuations in dispersing plumes. Environ Fluid Mech 9(3):341–357
33. Marro M, Salizzoni P, Cierco FX, Korsakissok I, Danzi E, Soulhac L (2014) Plume rise and spread in buoyant releases from elevated sources in the lower atmosphere. Environ Fluid Mech 14(1):201–219
34. Mavroidis I, Andronopoulos S, Venetsanos A, Bartzis JG (2015) Numerical investigation of concentrations and concentration fluctuations around isolated obstacles of different shapes. Comparison with wind tunnel results. Environ Fluid Mech 15(5):999–1034
35. Minier J-P, Chibbaro S, Pope SB (2014) Guidelines for the formulation of Lagrangian stochastic models for particle simulations of single-phase and dispersed two-phase turbulent flows. Phys Fluids 26(11):113303. https://doi.org/10.1063/1.4901315

36. Monin AS, Obukhov AM (1954) Basic laws of turbulent mixing in the surface layer of the atmosphere. Tr Akad Nauk SSSR Geophiz Inst 24(151):163–187
37. Osada N (2011) Height-dependent changes in shoot structure and tree allometry in relation to maximum height in four deciduous tree species. Funct Ecol 25:777–786. https://doi.org/10.1111/j.1365-2435.2011.01833.x
38. Ould-Dada Z (2002) Dry deposition profile of small particles within a model spruce canopy. Sci Total Environ 286:83–96
39. Ould-Dada Z, Copplestone D, Toal M, Shaw G (2002) Effect of forest edges on deposition of radioactive aerosols. Atmos Environ 36:5595–5606
40. Padro J, Hartog GD, Neumann HH (1991) An investigation of the ADOM dry deposition module using summertime O3 measurements above a deciduous forest. Atmos Environ 25A(8):1689–1704
41. Parker ST, Kinnersley RP (2004) A computational and wind tunnel study of particle dry deposition in complex topography. Atmos Environ 38:3867–3878
42. Pesava P, Aksu R, Toprak S, Horvath H, Seidl S (1999) Dry deposition of particles to building surfaces and soiling. Sci Total Environ 235:25–35
43. Petroff A, Mailliat A, Amielh M, Anselmet F (2008) Aerosol dry deposition on vegetative canopies. Part II: a new modelling approach and applications. Atmos Environ 42(16):3654–3683
44. Piskunov VN (2009) Parameterization of aerosol dry deposition velocities onto smooth and rough surfaces. Aerosol Sci 40:664–679
45. Pope SB (1998) The vanishing effect of molecular diffusivity on turbulent dispersion: implications for turbulent mixing and the scalar flux. J Fluid Mech 359:299–312
46. Qin H, Hong B, Jiang R, Yan S, Zhou Y (2019) The effect of vegetation enhancement on particulate pollution reduction: CFD simulations in an urban park. Forests 10:373. https://doi.org/10.3390/f10050373
47. Reinap A, Wiman BLB, Svenningsson B, Gunnarsson S (2012) Forest-edge effects on sea-salt aerosol deposition: a wind-tunnel study using living oak leaves. Boreal Environ Res 17:193–209
48. Roupsard P, Amielh M, Maro D, Coppalle A, Branger H, Connan O, Laguionie P, Hébert D, Talbaut M (2013) Measurement in a wind tunnel of dry deposition velocities of submicron aerosol with associated turbulence onto rough and smooth urban surfaces. J Aerosol Sci 55:12–24
49. Shaw G, Bailey E, Crout N, Field L, Freeman S, Gaschak S, Hou X, Izquierdo M, Wells C, Xu S, Young S (2019) Analysis of I-129 and I-127 in soils of the chernobyl exclusion zone, 29 years after the deposition of I-129. Sci Total Environ 692:966–974
50. Shaw G, Farrington-Smith JG, Kinnersley RP, Minski MJ (1994) Dry deposition of aerosol particles within model spruce canopies. Sci Total Environ 157:17–23
51. Tinarelli G, Anfossi D, Brusasca G, Ferrero E, Giostra U, Morselli MG, Moussafir J, Tampieri F, Trombetti F (1994) Lagrangian particle simulation of tracer dispersion in the lee of a schematic twodimensional hill. J Appl Meteorol 33:744–756
52. Sip V, Benes L (2017) Dry deposition model for a microscale aerosol dispersion solver based on the moment method. J Aerosol Sci 107:107–122
53. Soares-Frazão S, Lhomme J, Guinot V, Zech Y (2008) Two-dimensional shallow water model with porosity for urban flood modelling. J Hydraul Res 46(1):45–64
54. SPRAY-WEB (Università del Piemonte Orientale et al.); 2019; http://sprayweb.isac.cnr.it/
55. Thomson DJ (1987) Criteria for the selection of the stochastic models of particle trajectories in turbulent flows. J Fluid Mech 180:529–556
56. Vong RJ, Vong IJ, Vickers D, Covert DS (2010) Size-dependent aerosol deposition velocities during BEARPEX'07. Atmos Chem Phys 10:5749–5758
57. Zhang L, Gong S, Padro J, Barrie L (2001) A size-segregated particle dry deposition scheme for an atmospheric aerosol module. Atmos Environ 35(3):549–560
58. Zhang Z, Zhang D, Jiang X, Liu X (2014) Study on natural contamination performance of typical types of insulators. IEEE Trans Dielectr Electr Insul 21(4):1901–1909. https://doi.org/10.1109/TDEI.2014.004343

Authors and Affiliations

Andrea Amicarelli[1] · Stefano Alessandrini[1,2] · Giordano Agate[1] · Enrico Ferrero[3] · Guido Pirovano[1] · Gianni Luigi Tinarelli[4] · Silvia Trini Castelli[5]

✉ Andrea Amicarelli
andrea.amicarelli@rse-web.it

Stefano Alessandrini
alessand@ucar.edu

Giordano Agate
giordano.agate@rse-web.it

Enrico Ferrero
enrico.ferrero@uniupo.it

Guido Pirovano
guido.pirovano@rse-web.it

Gianni Luigi Tinarelli
g.tinarelli@aria-net.it

Silvia Trini Castelli
S.TriniCastelli@isac.cnr.it

[1] Department SFE, Ricerca sul Sistema Energetico - RSE SpA, via Rubattino, 54, 20134 Milan, Italy

[2] National Center for Atmospheric Research (NCAR), Boulder, CO, USA

[3] Dipartimento Di Scienze E Innovazione Tecnologica, Universita' del Piemonte Orientale, Alessandria, Italy

[4] ARIANET Srl, via Gilino 9, 20128 Milan, Italy

[5] Institute of Atmospheric Sciences and Climate, CNR, Corso Fiume 4, 10133 Torino, Italy